

NEW FINITE ELEMENT ITERATIVE METHODS FOR SOLVING A NONUNIFORM IONIC SIZE MODIFIED POISSON-BOLTZMANN EQUATION

DEXUAN XIE

Abstract. In this paper, a nonuniform size modified Poisson-Boltzmann equation (SMPBE) for a protein in a solvent with multiple ionic species in distinct ionic sizes is derived by using a new electrostatic free energy functional and solution decomposition techniques. It is then proved to have a unique solution, and the solution satisfies a system consisting of nonlinear algebraic equations and one Poisson dielectric interface problem. To solve it numerically, two new finite element iterative schemes are proposed by using nonlinear successive over-relaxation techniques, along with an improved uniform SMPBE for generating initial iterates. Furthermore, they are programmed in Python and Fortran as a software package for solving the nonuniform SMPBE, and numerically tested on a Born ball test model and a protein in a sodium chloride solution and a sodium chloride and potassium chloride solution. Numerical results confirm the convergence of the two new iterative schemes and demonstrate the high performance of the new software package.

Key words. Poisson-Boltzmann equation, finite element method, nonlinear successive over-relaxation, ionic size effects, electrostatics.

1. Introduction

The Poisson-Boltzmann equation (PBE) is one widely used implicit solvent model for electrostatics of ionic solvated biomolecules [24, 50]. It can produce solvent effects comparable to all-explicit-molecular models [7, 8, 16, 24, 44], and has been successively applied to the study of ionic solutions, biomolecular structure and function, catalytic activity, ligand association, protein docking, ion channel modeling, and rational drug design [2, 3, 4, 17, 19, 21, 24, 30, 34, 41, 48, 51, 52, 53]. Many PBE numerical algorithms, software packages, and web servers were developed in the last decades (see [5, 13, 15, 29, 40, 43, 49, 54] for examples). In the last five years, we developed PBE finite element solvers and software packages using our solution decomposition techniques [26, 37, 56, 57, 61], including one web server (sdpbs.math.uwm.edu) for the calculation of electrostatic solvation and binding free energies [27].

However, PBE distinguishes ions only by charge, so it may work poorly in applications that require distinguishing ions by size (e.g. Na^+ and K^+) [20, 25, 28, 31, 46]. To reflect ionic size effects, several dielectric continuum models were proposed (see the introduction of [47] for a short review, for example). In this paper, we only consider one of them — a size modified PBE (SMPBE).

So far, several SMPBE models were proposed as extensions of the early SMPBE proposed in 1997 [10], and solved numerically by finite difference and finite element algorithms [11, 14, 36, 42, 63]. One typical SMPBE was studied mathematically in [33, 35]. But, for SMPBE in the case of a protein in a solvent with multiple ionic species in distinct ionic sizes, which will be called *the nonuniform SMPBE* for clarity, there was only one finite difference algorithm publicly available, which worked for a case of three ionic species in two different ion sizes [14]. From a brief

review presented in the supplementation file of [55] it can be seen that this solver used a simple iteration scheme and did not deal with solution singularity by any solution decomposition technique. As another approach, a finite element scheme for solving a size modified Poisson-Nernst-Planck model (SMPNP) was used to solve the nonuniform SMPBE as the steady state of SMPNP [42].

Recently, we adapted our PBE finite element solver [56] to the numerical solution of SMPBE in the case of all ions having the same volumetric size, which will be called the uniform SMPBE [36]. This solver is now publicly available through the web server: smpbs.math.uwm.edu [59]. The key part of this solver is a solution decomposition scheme, which overcomes one major difficulty stemming from the solution singularity. We selected finite element techniques to solve SMPBE since they can be much more effective than finite difference techniques to deal with the complicated interface geometries and interface conditions. Based on our uniform SMPBE work [36, 56, 59], we intend to develop new finite element schemes for solving the nonuniform SMPBE in this paper.

Before doing so, we need to modify the current nonuniform SMPBE and its derivation to avoid their drawbacks. In fact, the current nonuniform SMPBE relied on a volume parameter of a water molecule and was derived from an electrostatic free energy functional involving the singular electrostatic potential function, the concentration of water molecules, and the volume of a water molecule [33, 42]. Since water molecules were treated as particles with sizes, various voids occurred among ions and water molecules, breaking down a size constraint condition required by the definition of SMPBE. To fix this drawback, a concentration of voids was introduced in [38]. But, this treatment required the representation of void volumes in one parameter, which is impossible since voids may have different shapes and volumes. Using the concentration of water molecules to derive SMPBE also caused a redundancy problem since the water solution had been treated as a continuum dielectric. On the other hand, the current electrostatic free energy functional was singular due to using the singular electrostatic potential function for its definition. To deal with the singularity issue, a complicated analysis had to be done to prove the solution existence and uniqueness of SMPBE [33, 34]. Hence, it is necessary to modify the current SMPBE and its derivation before we construct numerical algorithms.

To do so, we start with a revisit of the Poisson dielectric model using solution decomposition techniques. In order to use biochemical data directly in calculation, the Poisson dielectric model is reconstructed in dimensionless form by using ionic concentrations in moles per liter, lengths in angstroms, and other related parameters in SI units. Its solution u is then decomposed into three component functions (G , Ψ , and $\tilde{\Phi}$ as defined in Section 2.2) to deal with the singularity caused by atomic point charges. As illustrated in [58, see Figure 3, pp. 043304-9], the smaller the mesh size, the stronger such a singularity becomes. Hence, a solution decomposition technique becomes essential to overcome such a singular difficulty.

We make three changes to modify the current electrostatic free energy functionals as the new one in this paper. Firstly, we remove the concentration of water molecules and the volume of a water molecule to yield a modified size constraint condition (see (20)). Secondly, the singular potential u is replaced by the component function $\tilde{\Phi}$ to avoid singularity difficulties. Thirdly, bulk ionic concentrations are used directly in the ideal gas free energy term. Consequently, from a minimization of this new functional we derive a nonuniform SMPBE. Furthermore, we prove that the nonuniform SMPBE has a unique solution, and the solution satisfies a

system consisting of nonlinear algebraic equations and the Poisson dielectric model (see Theorem 2.1). Although our nonuniform SMPBE is slightly different from the current ones, its derivation and analysis are remarkably different from the current ones.

We next develop nonlinear iterative schemes for solving the nonuniform SMPBE using the classic nonlinear SOR (successive over-relaxation) iterative techniques [45]. The nonlinear SOR method was established in the 1950s to solve a large scale system of nonlinear algebraic equations arisen from numerical approximations to nonlinear elliptic boundary value problems [45]. It can be efficient for solving the nonuniform SMPBE since it can sharply reduce the computation complexity through separating each equation from the others. Each nonlinear algebraic equation of the nonuniform SMPBE system has the unknown functions — ionic concentration functions and electrostatic potential function. Based on the finite element approach, it is approximated as a system of nonlinear finite element equations with the unknowns being the mesh values of ionic concentration functions and electrostatic potential function on a mesh of the solvent domain. The equations of this system are independent each other so that this finite element system becomes a nonlinear equation of one unknown vector when it is solved numerically by the nonlinear SOR method. Using this special feature, in this paper, we construct a new nonlinear SOR-like scheme in vector form, and solve each related nonlinear equation by a Newton scheme iteratively until a convergence rule is satisfied. After the ionic concentration functions are updated, the Poisson dielectric model is solved by a finite element method to complete one iteration of the nonlinear SOR-like scheme. We also obtain the SOR-Newton scheme when each related nonlinear equation is solved by one Newton iteration only. From the nonlinear SOR convergence theory [45] it implies that our two nonlinear SOR schemes can have fast rates of convergence since the size of a nonuniform SMPBE system is small, typically 3 or 4 for applications involving two or three ionic species.

As iterative methods, our nonlinear SOR-like and SOR-Newton schemes require initial iterates. A good selection of initial iterate can improve the convergence and performance of our two schemes significantly. For this purpose, in this paper, we propose an improved uniform SMPBE by setting the volume of each ion to be the average of ion volumes. In contrast, in the uniform SMPBE, the ions are set to have the volume of a water molecule. Clearly, the improved uniform SMPBE can better approximate the nonuniform SMPBE than the uniform SMPBE so that it can produce better initial iterates for our two iterative schemes.

We programmed our new nonuniform SMPBE finite element solvers in Python and Fortran as a software package based on the state-of-the-art finite element library from the FEniCS project [39], the linear algebra library NumPy (www.numpy.org), and our PBE and uniform SMPBE program packages [27, 56, 59]. We also extended our uniform SMPBE program package to make it work for a solvent with any number of ionic species. We then adapted it to the numerical solution of the improved uniform SMPBE for the generation of initial iterates. To demonstrate the performance of the new nonuniform SMPBE software, we did numerical tests on a Born ball test model and a protein with 892 atoms for a solution of sodium chloride (NaCl, table salt) and a solution of sodium chloride and potassium chloride (NaCl-KCl), respectively. Numerical results validated our nonuniform SMPBE, confirmed the convergence of our two nonlinear SOR schemes, and demonstrated the high performance of our software package.

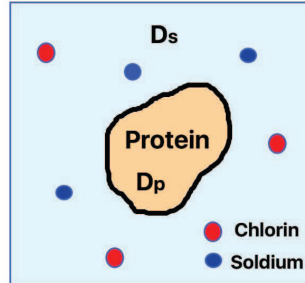


FIGURE 1. An illustration of a protein region D_p surrounded by a solvent region D_s with sodium ions (Na^+) and chloride ions (Cl^-).

The remaining part of the paper is arranged as follows. In Section 2, we construct and analyze the nonuniform SMPBE. In Section 3, we present new nonuniform SMPBE finite element solvers. In Section 4, we present an improved uniform SMPBE. In Section 5, we report the SMPBE program package and numerical results. Finally, conclusions are made in Section 6.

2. Derivation of the nonuniform SMPBE

In this section, we first derive the Poisson dielectric model and its solution decomposition as a general framework for developing dielectric continuum models for protein in ionic solvent. We then derive the nonuniform SMPBE using a new electrostatic free energy functional. Moreover, we prove that the nonuniform SMPBE has a unique solution, and the solution satisfies a system of nonlinear algebraic equations and one Poisson dielectric model.

2.1. Poisson dielectric model. Let a protein with n_p atoms be wrapped by a molecular surface Γ to form a protein region D_p , and \mathbf{r}_j and z_j denote the position and charge number of atom j . For a sufficiently large domain Ω (a rectangular box or a sphere), a water solution region D_s is set as $D_s = \Omega \setminus (D_p \cup \Gamma)$, and contains n different ionic species. We assume that a boundary value function, g , is known on the boundary $\partial\Omega$ of Ω . For example, g is simply set as zero due to the fact that $\Phi(\mathbf{r}) \rightarrow 0$ as the length $|\mathbf{r}| \rightarrow \infty$ for $\mathbf{r} = (x, y, z) \in \mathbb{R}^3$. Other selections of g can be found in [23, 41]. See Figure 1 for an illustration, and Figures 3 and 4 for examples of molecular surface Γ and domain Ω .

As usual, we estimate the charge density functions, ρ_p and ρ_s , within D_p and D_s by the expressions

$$(1) \quad \rho_p(\mathbf{r}) = e_c \sum_{j=1}^{n_p} z_j \delta_{\mathbf{r}_j}, \quad \mathbf{r} \in D_p; \quad \rho_s(\mathbf{r}) = e_c \sum_{i=1}^n Z_i c_i(\mathbf{r}), \quad \mathbf{r} \in D_s,$$

where c_i and Z_i denote the concentration function and charge number of the i -th ionic species, respectively, $\delta_{\mathbf{r}_j}$ is the Dirac delta distribution at \mathbf{r}_j , and e_c is the elementary charge. Based on the implicit solvent approach [24, 50] and the classic linear dielectric theory [18, 22], D_p and D_s are treated as dielectric continuum media with relative permittivity constants ϵ_p and ϵ_s so that the electrostatic potential function Φ within D_p and D_s can be estimated, respectively, by the Poisson

equations

$$(2) \quad -\epsilon_0\epsilon_p\Delta\Phi(\mathbf{r}) = e_c \sum_{j=1}^{n_p} z_j\delta_{\mathbf{r}_j}, \quad \mathbf{r} \in D_p.$$

and

$$(3) \quad -\epsilon_0\epsilon_s\Delta\Phi(\mathbf{r}) = e_c \sum_{i=1}^n Z_i c_i(\mathbf{r}), \quad \mathbf{r} \in D_s,$$

where ϵ_0 is the permittivity of the vacuum.

To merge (2) and (3) together as a dielectric model for estimating Φ in the whole domain Ω , it is natural to require that Φ is continuous across the interface Γ :

$$(4) \quad \Phi(\mathbf{s}^-) = \Phi(\mathbf{s}^+), \quad \mathbf{s} \in \Gamma,$$

where $\Phi(\mathbf{s}^\pm) = \lim_{t \rightarrow 0^\pm} \Phi(\mathbf{s} \pm t\mathbf{n}(\mathbf{s}))$ with $\mathbf{n}(\mathbf{s})$ being the unit outward normal vector of D_p . From the classic linear dielectric theory [22] it is known that ρ_p and ρ_s induce displacement fields, \mathbf{d}_p and \mathbf{d}_s , respectively, as follows:

$$\nabla \cdot \mathbf{d}_p(\mathbf{r}) = \rho_p(\mathbf{r}) \quad \forall \mathbf{r} \in D_p; \quad \nabla \cdot \mathbf{d}_s(\mathbf{r}) = \rho_s(\mathbf{r}) \quad \forall \mathbf{r} \in D_s,$$

and \mathbf{d}_p and \mathbf{d}_s are continuous across the interface Γ :

$$(5) \quad \mathbf{d}_p(\mathbf{s}^-) \cdot \mathbf{n}(\mathbf{s}) = \mathbf{d}_s(\mathbf{s}^+) \cdot \mathbf{n}(\mathbf{s}) \quad \forall \mathbf{s} \in \Gamma.$$

From (2) and (3) we can get that

$$(6) \quad \mathbf{d}_p(\mathbf{r}) = -\epsilon_0\epsilon_p\nabla\Phi(\mathbf{r}), \quad \mathbf{r} \in D_p; \quad \mathbf{d}_s(\mathbf{r}) = -\epsilon_0\epsilon_s\nabla\Phi(\mathbf{r}), \quad \mathbf{r} \in D_s.$$

Hence, applying (6) to (5) gives the second interface condition

$$(7) \quad \epsilon_s \frac{\partial\Phi(\mathbf{s}^+)}{\partial\mathbf{n}(\mathbf{s})} = \epsilon_p \frac{\partial\Phi(\mathbf{s}^-)}{\partial\mathbf{n}(\mathbf{s})} \quad \forall \mathbf{s} \in \Gamma,$$

where $\frac{\partial\Phi(\mathbf{s})}{\partial\mathbf{n}(\mathbf{s})} = \nabla\Phi(\mathbf{s}) \cdot \mathbf{n}(\mathbf{s})$. Consequently, a combination of the two Poisson equations (2) and (3) with the interface conditions (4) and (7) results in the Poisson dielectric model for protein in ionic solvent as follows:

$$(8) \quad \left\{ \begin{array}{ll} -\epsilon_0\epsilon_p\Delta\Phi(\mathbf{r}) = e_c \sum_{j=1}^{n_p} z_j\delta_{\mathbf{r}_j}, & \mathbf{r} \in D_p, \\ -\epsilon_0\epsilon_s\Delta\Phi(\mathbf{r}) = e_c \sum_{i=1}^n Z_i c_i(\mathbf{r}), & \mathbf{r} \in D_s, \\ \Phi(\mathbf{s}^-) = \Phi(\mathbf{s}^+), \quad \epsilon_s \frac{\partial\Phi(\mathbf{s}^+)}{\partial\mathbf{n}(\mathbf{s})} = \epsilon_p \frac{\partial\Phi(\mathbf{s}^-)}{\partial\mathbf{n}(\mathbf{s})}, & \mathbf{s} \in \Gamma, \\ \Phi(\mathbf{s}) = g(\mathbf{s}), & \mathbf{s} \in \partial\Omega. \end{array} \right.$$

In the above model, we have used the SI (Système International) unit system to measure potential Φ in volts (V), length in meters (m), and concentration c_i in the number of ions per cubic meter. The parameters e_c and ϵ_0 are estimated by

$$e_c = 1.602176565 \times 10^{-19} \text{ C}, \quad \epsilon_0 = 8.854187817 \times 10^{-12} \text{ F/m},$$

where C and F denote Coulomb (the unit of electric charge) and Farad (the unit of capacitance), respectively. See <http://physics.nist.gov/cuu/Constants/index.html> for the updating of the physical parameters.

But, in biomolecular simulation, the length unit is angstrom (\AA), and c_i in moles per liter (mol/L). Hence, we change the units of ϵ_0 and c_i as shown below:

$$(9) \quad \epsilon_0 \text{ F/m} = \frac{\epsilon_0}{10^{10}} \text{ F/\AA}, \quad c_i \text{ mol/L} = c_i 10^3 N_A / m^3 = 10^{-27} N_A c_i / \text{\AA}^3,$$

where we have used the unit converters: $1 \text{ m} = 10^{10} \text{ \AA}$, and $1 \text{ L} = m^3/10^3$, and the Avogadro number $N_A = 6.02214129 \times 10^{23}$, which estimates the number of ions per mole. Furthermore, the Poisson dielectric model (8) is often rescaled to a dimensionless form by using the variable change

$$(10) \quad u = \frac{e_c}{k_B T} \Phi,$$

where k_B is the Boltzmann constant, and T is the absolute temperature. In the SI system, $k_B = 1.380648813 \times 10^{-23}$ Joule/Kelvin (J/K) at $T = 298.15$ K. Since $1 \text{ V} = 1 \text{ J/C}$, the factor $\frac{e_c}{k_B T}$ is in $1/\text{V}$. Thus, u becomes dimensionless. Hence, when the length unit is in \AA , and each c_i in mol/L, by (9) and (10), the Poisson dielectric model (8) can be rescaled to the dimensionless form

$$(11) \quad \begin{cases} -\epsilon_p \Delta u(\mathbf{r}) = \alpha \sum_{j=1}^{n_p} z_j \delta_{\mathbf{r}_j}, & \mathbf{r} \in D_p, \\ -\epsilon_s \Delta u(\mathbf{r}) = \beta \sum_{i=1}^n Z_i c_i(\mathbf{r}), & \mathbf{r} \in D_s, \\ u(\mathbf{s}^-) = u(\mathbf{s}^+), \quad \epsilon_s \frac{\partial u(\mathbf{s}^+)}{\partial \mathbf{n}(\mathbf{s})} = \epsilon_p \frac{\partial u(\mathbf{s}^-)}{\partial \mathbf{n}(\mathbf{s})}, & \mathbf{s} \in \Gamma, \\ u(\mathbf{s}) = \hat{g}(\mathbf{s}), & \mathbf{s} \in \partial\Omega, \end{cases}$$

where α , β , and \hat{g} are defined by

$$(12) \quad \alpha = \frac{10^{10} e_c^2}{\epsilon_0 k_B T}, \quad \beta = \frac{N_A e_c^2}{10^{17} \epsilon_0 k_B T}, \quad \hat{g} = \frac{e_c}{k_B T} g.$$

At $T = 298.15$, we can estimate α , β , and $\frac{e_c}{k_B T}$ in the following values:

$$\alpha \approx 7042.93990033, \quad \beta \approx 4.24135792, \quad \frac{e_c}{k_B T} \approx 38.92174809.$$

When the solution u is found, we can gain Φ by (10) for energy calculation.

2.2. Solution decomposition. However, the Poisson dielectric model (11) is difficult to study due to the solution singularity caused by the distributions $\delta_{\mathbf{r}_j}$. To avoid such a difficulty, we split the solution u in the form

$$(13) \quad u(\mathbf{r}) = G(\mathbf{r}) + \Psi(\mathbf{r}) + \tilde{\Phi}(\mathbf{r}) \quad \forall \mathbf{r} \in \Omega,$$

where G is given by

$$(14) \quad G(\mathbf{r}) = \frac{\alpha}{4\pi\epsilon_p} \sum_{j=1}^{n_p} \frac{z_j}{|\mathbf{r} - \mathbf{r}_j|},$$

Ψ is a solution of the linear interface problem

$$(15) \quad \begin{cases} \Delta \Psi(\mathbf{r}) = 0, & \mathbf{r} \in D_p \cup D_s, \\ \Psi(\mathbf{s}^+) = \Psi(\mathbf{s}^-), \quad \epsilon_s \frac{\partial \Psi(\mathbf{s}^+)}{\partial \mathbf{n}(\mathbf{s})} = \epsilon_p \frac{\partial \Psi(\mathbf{s}^-)}{\partial \mathbf{n}(\mathbf{s})} + (\epsilon_p - \epsilon_s) \frac{\partial G(\mathbf{s})}{\partial \mathbf{n}(\mathbf{s})}, & \mathbf{s} \in \Gamma, \\ \Psi(\mathbf{s}) = \hat{g}(\mathbf{s}) - G(\mathbf{s}), & \mathbf{s} \in \partial\Omega, \end{cases}$$

and $\tilde{\Phi}$ is a solution of the interface problem

$$(16) \quad \begin{cases} \Delta \tilde{\Phi}(\mathbf{r}) = 0, & \mathbf{r} \in D_p, \\ -\epsilon_s \Delta \tilde{\Phi}(\mathbf{r}) = \beta \sum_{i=1}^n Z_i c_i(\mathbf{r}), & \mathbf{r} \in D_s, \\ \tilde{\Phi}(\mathbf{s}^+) = \tilde{\Phi}(\mathbf{s}^-), \quad \epsilon_s \frac{\partial \tilde{\Phi}(\mathbf{s}^+)}{\partial \mathbf{n}(\mathbf{s})} = \epsilon_p \frac{\partial \tilde{\Phi}(\mathbf{s}^-)}{\partial \mathbf{n}(\mathbf{s})}, & \mathbf{s} \in \Gamma, \\ \tilde{\Phi}(\mathbf{s}) = 0, & \mathbf{s} \in \partial\Omega. \end{cases}$$

Here $\frac{\partial G(\mathbf{s})}{\partial \mathbf{n}(\mathbf{s})} = \nabla G(\mathbf{s}) \cdot \mathbf{n}(\mathbf{s})$ with ∇G being given by

$$(17) \quad \nabla G(\mathbf{s}) = -\frac{\alpha}{4\pi\epsilon_p} \sum_{j=1}^{n_p} z_j \frac{(\mathbf{s} - \mathbf{r}_j)}{|\mathbf{s} - \mathbf{r}_j|^3}.$$

Clearly, G , Ψ , and $\tilde{\Phi}$ correspond to the electrostatic contributions from the protein domain D_p , the interface Γ , and the solvent domain D_s , respectively. Specially, the sum $\Psi + G$ gives the electrostatic potential for protein in water. Because G contains all the singular points of u , both Ψ and $\tilde{\Phi}$ become well defined without any singularity.

Following what is done in [57, Theorem 3.2], we can prove that (15) and (16) have unique solutions for $c_i \in L^2(\Omega)$, from which it implies the solution existence and uniqueness of the Poisson dielectric model (11). Here, c_i has been set as zero in D_p , and $L^2(\Omega)$ is the function space with the inner product $(u, v) = \int_{\Omega} uv d\mathbf{r}$ and the norm $\|v\| = \sqrt{\int_{\Omega} v^2 d\mathbf{r}}$.

2.3. Optimal selection of ionic concentrations. Clearly, different selections of ionic concentration functions may yield different electrostatic potential functions. To search for an optimal selection that can reflect ionic size effects, we first construct an ionic size constraint condition.

Let V , N_i , and v_i denote the volume of D_s , the number of ions of species i , and the volume of an ion of species i , respectively. Then, the volume occupied by the water solution, V_w , can be expressed by

$$(18) \quad V_w = V - \sum_{i=1}^n v_i N_i.$$

The average volume fraction ξ^b of the water solution in D_s and the bulk concentrations c_i^b are defined by

$$\xi^b = V_w/V, \quad c_i^b = N_i/V, \quad i = 1, 2, \dots, n.$$

Dividing by V on the both sides of (18), we find that

$$(19) \quad \xi^b = 1 - \sum_{i=1}^n v_i c_i^b.$$

We then generalize (19) as the ionic size constraint condition:

$$(20) \quad \xi(\mathbf{r}) + \sum_{i=1}^n v_i c_i(\mathbf{r}) = 1, \quad \mathbf{r} \in D_s,$$

where $\xi(\mathbf{r})$ denotes the volume fraction function of the water solution. Here c_i^b and c_i have units in the number of ions per \AA^3 when v_i is in \AA^3 .

In molecular calculation, ionic concentrations are usually given in units mol/L. Thus, for the convenience of calculation, we use (9) to rescale (20) as

$$(21) \quad \xi(\mathbf{r}) = 1 - \gamma \sum_{i=1}^n v_i c_i(\mathbf{r}), \quad \mathbf{r} \in D_s,$$

where $\gamma = 10^{-27} N_A$, which is estimated by

$$(22) \quad \gamma \approx 6.02214129 \times 10^{-4}.$$

We next consider an optimal selection of ionic concentrations under the size constraint condition (21) with $c = (c_1, c_2, \dots, c_n)$ and the bulk concentrations c_i^b

for $i = 1, 2, \dots, n$ being given in moles per liter. Using the solution decomposition (13), we construct a new electrostatic free energy functional, F , as follows:

$$(23) \quad F(c, \tilde{\Phi}) = F_{es}(c, \tilde{\Phi}) + F_{id}(c) + F_{ex}(c),$$

where F_{es} , F_{id} , and F_{ex} denote the electrostatic, ideal gas, and excess energies, respectively, which are defined in the following expressions

$$\begin{aligned} F_{es}(c, \tilde{\Phi}) &= \frac{k_B T}{2} \sum_{j=1}^{n_p} z_j \tilde{\Phi}(\mathbf{r}_j) + \frac{k_B T}{2} \gamma \sum_{i=1}^n Z_i \int_{D_s} (\tilde{\Phi} + \Psi + G) c_i d\mathbf{r}, \\ F_{id}(c) &= k_B T \gamma \sum_{i=1}^n \int_{D_s} c_i \left(\ln \frac{c_i}{c_i^b} - 1 \right) d\mathbf{r}, \\ F_{ex}(c) &= \frac{k_B T}{v_0} \int_{D_s} \left[1 - \gamma \sum_{i=1}^n v_i c_i(\mathbf{r}) \right] \left[\ln \left(1 - \gamma \sum_{i=1}^n v_i c_i(\mathbf{r}) \right) - 1 \right] d\mathbf{r}. \end{aligned}$$

Here v_0 is a size scaling parameter to give F_{ex} an energy unit. For example, we often set $v_0 = \min_{1 \leq i \leq n} v_i$ in calculation. The excess energy F_{ex} reflects the ionic size effects caused by the constraint condition (21).

Clearly, by the first Green's formula, the boundary value problem (16) can be reformulated as the variational problem:

$$(24) \quad \text{Find } \tilde{\Phi} \in H_0^1(\Omega) \text{ such that } a(\tilde{\Phi}, v) = b(v) \quad \forall v \in H_0^1(\Omega),$$

where $b(v) = \beta \sum_{i=1}^n Z_i \int_{D_s} c_i v d\mathbf{r}$, $a(u, v)$ is defined by

$$(25) \quad a(u, v) = \epsilon_p \int_{D_p} \nabla u \cdot \nabla v d\mathbf{r} + \epsilon_s \int_{D_s} \nabla u \cdot \nabla v d\mathbf{r},$$

and $H_0^1(\Omega) = \{v \in H^1(\Omega) \mid v(\mathbf{s}) = 0 \ \forall \mathbf{s} \in \partial\Omega\}$ with $H^1(\Omega)$ being the normal Sobolev space of functions with first order weak derivatives [1].

We next define linear operator, L , by

$$\langle Lu, v \rangle = a(u, v) \quad \forall v \in H_0^1(\Omega) \text{ for each } u \in H_0^1(\Omega),$$

so that the variational form (24) can be written in the operator equation

$$(26) \quad L\tilde{\Phi} - \beta \sum_{j=1}^n Z_j c_j = 0.$$

We now define an optimal c as a solution of the following Poisson dielectric equation constrained minimization problem:

$$(27) \quad \min\{F(c, \tilde{\Phi}) \mid (c, \tilde{\Phi}) \text{ satisfies (26) for } c \in [L^2(\Omega)]^n, \tilde{\Phi} \in H_0^1(\Omega)\},$$

where c_i has been set to be zero in D_p and continuous in D_s to ensure $c_i \in L^2(\Omega)$.

The main results are reported in Theorem 2.1.

Theorem 2.1. *The constrained minimization problem (27) has a unique minimizer, $(c, \tilde{\Phi})$, defined implicitly by a system of $n + 1$ equations as follows:*

$$(28) \quad c_i - c_i^b \left[1 - \gamma \sum_{j=1}^n v_j c_j \right]^{\frac{v_i}{v_0}} e^{-Z_i(\tilde{\Phi} + \Psi + G)} = 0, \quad i = 1, 2, \dots, n,$$

and the operator equation (26). Here γ is given in (22).

Proof. As what was done in [57], the variational problem (24) can be shown to have a unique solution, and the solution can be expressed as

$$(29) \quad \tilde{\Phi} = \tilde{\Phi}(c) \quad \text{with} \quad \tilde{\Phi}(c) = \beta \sum_{i=1}^n Z_i L^{-1} c_i,$$

where L^{-1} denotes the inverse of linear operator L , which is continuous self-adjoint positive. Thus, the electrostatic energy F_{es} can be reformulated as

$$\begin{aligned} F_{es}(c) &= \frac{k_B T}{2} \left[\sum_{j=1}^{n_p} z_j \tilde{\Phi}(c)(\mathbf{r}_j) + \gamma \sum_{i=1}^n Z_i \int_{D_s} (\Psi + G) c_i d\mathbf{r} \right. \\ &\quad \left. + \beta \gamma \sum_{i,j=1}^n Z_i Z_j \int_{\Omega} L^{-1} c_i c_j d\mathbf{r} \right]. \end{aligned}$$

Recall that $u = \tilde{\Phi} + \Psi + G$. We can find the first and second Fréchet derivatives of F_{id} , F_{es} , and F_{ex} as follows:

$$\begin{aligned} \frac{\partial F_{id}(c)}{\partial c_i} &= k_B T \gamma \ln \left(\frac{c_i}{c_i^b} \right), \quad \frac{\partial^2 F_{id}(c)}{\partial c_j \partial c_i} = \begin{cases} \frac{k_B T}{c_i} \gamma & j = i, \\ 0 & j \neq i, \end{cases} \\ \frac{\partial F_{es}(c)}{\partial c_i} &= k_B T \gamma Z_i u, \quad \frac{\partial^2 F_{es}(c)}{\partial c_j \partial c_i} = k_B T \gamma \beta Z_i Z_j L^{-1}, \\ \frac{\partial F_{ex}(c)}{\partial c_i} &= -k_B T \gamma \frac{v_i}{v_0} \ln \left(1 - \gamma \sum_{k=1}^n v_k c_k \right), \\ \frac{\partial^2 F_{ex}(c)}{\partial c_j \partial c_i} &= \frac{k_B T \gamma^2 v_i v_j}{v_0 \left(1 - \gamma \sum_{k=1}^n v_k c_k \right)}. \end{aligned}$$

Combining the above partial derivatives together, we get the first Fréchet derivative F' in the expression

$$F'(c)w = k_B T \gamma \sum_{i=1}^n \int_{D_s} \left[Z_i u + \ln \left(\frac{c_i}{c_i^b} \right) - \frac{v_i}{v_0} \ln \left(1 - \gamma \sum_{j=1}^n v_j c_j \right) \right] w_i(\mathbf{r}) d\mathbf{r},$$

where $w = (w_1, w_2, \dots, w_n)$ with $w_i \in L^2(\Omega)$.

From the stationary equation $F'(c)w = 0$ we obtain the n equations:

$$(30) \quad Z_i u + \ln \left(\frac{c_i}{c_i^b} \right) - \frac{v_i}{v_0} \ln \left(1 - \gamma \sum_{j=1}^n v_j c_j \right) = 0, \quad i = 1, 2, \dots, n,$$

from which we obtain the expressions of (28).

Furthermore, we can obtain the second Fréchet derivative F'' as below:

$$\begin{aligned} F''(c)(w, w) &= k_B T \beta \gamma \left\langle L^{-1} \sum_{i=1}^n Z_i w_i, \sum_{i=1}^n Z_i w_i \right\rangle \\ &\quad + k_B T \gamma \sum_{i=1}^n \int_{D_s} \frac{1}{c_i} (w_i(\mathbf{r}))^2 d\mathbf{r} \\ &\quad + \frac{k_B T}{v_0} \gamma^2 \int_{D_s} \frac{1}{1 - \gamma \sum_{i=1}^n v_i c_i} \left(\sum_{i=1}^n v_i w_i \right)^2 d\mathbf{r}. \end{aligned}$$

From the above expression we see that $F''(c)$ is strictly positive for any $w \neq 0$, implying that the minimization problem (27) has a unique solution. This completes the proof. \square

Corollary 2.2. *Let $u = \tilde{\Phi} + \Psi + G$. If the ion volumes $v_i = v_0$ for $i = 1, 2, \dots, n$, then each concentration c_i can be expressed as an explicit function of u as follows:*

$$(31) \quad c_i(\mathbf{r}) = \frac{c_i^b e^{-Z_i u(\mathbf{r})}}{1 + v_0 \gamma \sum_{j=1}^n c_j^b e^{-Z_j u(\mathbf{r})}}, \quad i = 1, 2, \dots, n.$$

Specifically, if $v_0 = 0$, the above c_i is reduced to the classic Boltzmann distribution

$$(32) \quad c_i(\mathbf{r}) = c_i^b e^{-Z_i u(\mathbf{r})}, \quad i = 1, 2, \dots, n.$$

Proof. When $v_i = v_0$ for $i = 1, 2, \dots, n$, the equations of (28) are simplified as

$$(33) \quad c_i = c_i^b \left[1 - v_0 \gamma \sum_{j=1}^n c_j(\mathbf{r}) \right] e^{-Z_i u(\mathbf{r})}, \quad i = 1, 2, \dots, n.$$

Summarizing the above equations from their both sides gives

$$\sum_{i=1}^n c_i(\mathbf{r}) = \left[1 - v_0 \gamma \sum_{j=1}^n c_j(\mathbf{r}) \right] \sum_{i=1}^n c_i^b e^{-Z_i u(\mathbf{r})},$$

from which we can get

$$\sum_{i=1}^n c_i(\mathbf{r}) = \frac{\sum_{i=1}^n c_i^b e^{-Z_i u(\mathbf{r})}}{1 + v_0 \gamma \sum_{i=1}^n c_i^b e^{-Z_i u(\mathbf{r})}}.$$

We substitute the above expression to (33) to gain (31). It is obvious that the equations of (28) is reduced to (32) when $v_0 = 0$. This completes the proof. \square

2.4. The nonuniform SMPBE for protein in ionic solvent. According to Theorem 2.1, we define the nonuniform SMPBE as a system of $n + 1$ equations, which contains one linear interface boundary value problem,

$$(34) \quad \begin{cases} -\epsilon_p \Delta u(\mathbf{r}) = \alpha \sum_{j=1}^{n_p} z_j \delta_{\mathbf{r}_j}, & \mathbf{r} \in D_p, \\ -\epsilon_s \Delta u(\mathbf{r}) = \beta \sum_{i=1}^n Z_i c_i(\mathbf{r}), & \mathbf{r} \in D_s, \\ u(\mathbf{s}^-) = u(\mathbf{s}^+), \quad \epsilon_s \frac{\partial u(\mathbf{s}^+)}{\partial \mathbf{n}(\mathbf{s})} = \epsilon_p \frac{\partial u(\mathbf{s}^-)}{\partial \mathbf{n}(\mathbf{s})}, & \mathbf{s} \in \Gamma, \\ u(\mathbf{s}) = \hat{g}(\mathbf{s}), & \mathbf{s} \in \partial\Omega, \end{cases}$$

and n nonlinear algebraic equations:

$$(35) \quad c_i(\mathbf{r}) - c_i^b \left[1 - \gamma \sum_{j=1}^n v_j c_j(\mathbf{r}) \right]^{\frac{v_i}{v_0}} e^{-Z_i u(\mathbf{r})} = 0, \quad i = 1, 2, \dots, n.$$

Here α , β , \hat{g} , and γ are given in (12) and (22). The solution of the nonuniform SMPBE gives n optimal ionic concentration functions c_i for $i = 1, 2, \dots, n$ and one related electrostatic potential u in the sense of minimizing the electrostatic free energy functional F of (23).

Specifically, when all the ionic volumes $v_i = v_0$ for $i = 1, 2, \dots, n$, applying (31) to (34), we obtain the uniform SMPBE:

$$(36) \quad \left\{ \begin{array}{ll} -\epsilon_p \Delta u(\mathbf{r}) = \alpha \sum_{j=1}^{n_p} z_j \delta_{\mathbf{r}_j}, & \mathbf{r} \in D_p, \\ \epsilon_s \Delta u(\mathbf{r}) + \beta \frac{\sum_{i=1}^n Z_i c_i^b e^{-Z_i u(\mathbf{r})}}{1 + v_0 \gamma \sum_{i=1}^n c_i^b e^{-Z_i u(\mathbf{r})}} = 0, & \mathbf{r} \in D_s, \\ u(\mathbf{s}^-) = u(\mathbf{s}^+), \quad \epsilon_s \frac{\partial u(\mathbf{s}^+)}{\partial \mathbf{n}(\mathbf{s})} = \epsilon_p \frac{\partial u(\mathbf{s}^-)}{\partial \mathbf{n}(\mathbf{s})}, & \mathbf{s} \in \Gamma, \\ u(\mathbf{s}) = \hat{g}(\mathbf{s}), & \mathbf{s} \in \partial\Omega. \end{array} \right.$$

Without considering any ionic size effect, we set $v_0 = 0$ to reduce the uniform SMPBE into the classic PBE:

$$(37) \quad \left\{ \begin{array}{ll} -\epsilon_p \Delta u(\mathbf{r}) = \alpha \sum_{j=1}^{n_p} z_j \delta_{\mathbf{r}_j}, & \mathbf{r} \in D_p, \\ \epsilon_s \Delta u(\mathbf{r}) + \beta \sum_{i=1}^n Z_i c_i^b e^{-Z_i u(\mathbf{r})} = 0, & \mathbf{r} \in D_s, \\ u(\mathbf{s}^-) = u(\mathbf{s}^+), \quad \epsilon_s \frac{\partial u(\mathbf{s}^+)}{\partial \mathbf{n}(\mathbf{s})} = \epsilon_p \frac{\partial u(\mathbf{s}^-)}{\partial \mathbf{n}(\mathbf{s})}, & \mathbf{s} \in \Gamma, \\ u(\mathbf{s}) = \hat{g}(\mathbf{s}), & \mathbf{s} \in \partial\Omega. \end{array} \right.$$

Hence, the nonuniform SMPBE contains both the uniform SMPBE and the classic PBE as two special cases.

Clearly, the algebraic equations of (35) is well defined only if

$$0 \leq \xi(\mathbf{r}) \leq 1 \quad \forall \mathbf{r} \in D_s \quad \text{with } \xi(\mathbf{r}) = 1 - \gamma \sum_{j=1}^n v_j c_j(\mathbf{r}).$$

In fact, it is true that $\xi(\mathbf{r}) \leq 1$ since all $c_i \geq 0$. In Physics, it is obvious that $\xi \geq 0$ since ξ stands for the volume fraction of the water solution, which is always much larger than the volume occupied by the ions in D_s . But, in numerical calculation, negative values of ξ may occur when an initial iterate is a poor approximation to the solution of SMPBE, causing an iterative process for a numerical solution to crash.

To ensure that $\xi(\mathbf{r}) \geq 0$, we present a sufficient condition in Theorem 2.3.

Theorem 2.3. *If concentration functions c_j satisfy the range constraints*

$$(38) \quad 0 \leq c_j(\mathbf{r}) \leq \frac{1}{\gamma \sum_{i=1}^n v_i} \quad \forall \mathbf{r} \in D_s, \quad j = 1, 2, \dots, n,$$

then $1 - \gamma \sum_{j=1}^n v_j c_j(\mathbf{r}) \geq 0$ in D_s .

Proof. Under the conditions of (38), it is clear that

$$\max_{1 \leq j \leq n} \max_{\mathbf{r} \in \Omega} c_j(\mathbf{r}) \leq \frac{1}{\gamma \sum_{i=1}^n v_i}.$$

Thus, we can get

$$\sum_{i=1}^n v_i c_i(\mathbf{r}) \leq \sum_{i=1}^n v_i \max_{\mathbf{r} \in \Omega} c_i(\mathbf{r}) \leq \max_{1 \leq i \leq n} \max_{\mathbf{r} \in \Omega} c_i(\mathbf{r}) \sum_{i=1}^n v_i \leq \frac{1}{\gamma}.$$

Hence, $\gamma \sum_{j=1}^n v_j c_j(\mathbf{r}) \leq 1$, implying that $1 - \gamma \sum_{j=1}^n v_j c_j(\mathbf{r}) \geq 0$. This completes the proof. \square

3. New finite element solvers for nonuniform SMPBE

In this section, we construct two new finite element solvers for the nonuniform SMPBE by the solution decomposition of (13). Since G and Ψ have been calculated efficiently in [56], we only consider the following system for computing $\tilde{\Phi}$ and c_i :

$$(39) \quad \begin{cases} c_i - c_i^b w_i \left[1 - \gamma \sum_{j=1}^n v_j c_j \right]^{\frac{v_i}{v_0}} e^{-Z_i \tilde{\Phi}} = 0, & i = 1, 2, \dots, n, \\ L\tilde{\Phi} - \beta \sum_{j=1}^n Z_j c_j = 0, \end{cases}$$

where β is given in (12), and $w_i = e^{-Z_i(\Psi+G)}$, which has been calculated. In calculation, the operator equation is solved as the variational problem (24).

Let \mathcal{M} denote a Lagrange finite element function space constructed on an interface fitted irregular tetrahedral mesh Ω_h of Ω . See Figures 3 and 4 for examples of our interface triangular meshes and mesh domain Ω_h . We assume that \mathcal{M} is a finite dimensional subspace of the Sobolev function space $H^1(\Omega)$ [12], and each function of \mathcal{M} is continuous in both D_p and D_s . We also set $\mathcal{M}_0 = \{v \in \mathcal{M} | v = 0 \text{ on } \partial\Omega\}$ as a subspace of $H_0^1(\Omega)$. We then discretize the system (39) as a system of $(n + 1)N_h$ finite element equations such that $\tilde{\Phi} \in \mathcal{M}_0$ and $c_i \in \mathcal{M}$ for $i = 1, 2, \dots, n$. Here N_h denotes the total number of mesh vertices of Ω_h .

To sharply reduce the computer memory requirement, we construct a nonlinear SOR-like iterative scheme for solving the finite element system in a block form. Here each block corresponds to one finite element function on \mathcal{M} .

Let $\bar{c}^{(k)} = (c_1^{(k)}, c_2^{(k)}, \dots, c_n^{(k)}, \tilde{\Phi}^{(k)})$ denote the k th iterate of the nonlinear SOR-like scheme with $\tilde{\Phi}^{(k)} \in \mathcal{M}_0$ and $c_i^{(k)} \in \mathcal{M}$. When $\bar{c}^{(0)}$ is given, we update $\bar{c}^{(k)}$ for $k \geq 0$ by the formulas

$$(40) \quad c_i^{(k+1)}(\mathbf{r}) = c_i^{(k)}(\mathbf{r}) + \omega [p_i(\mathbf{r}) - c_i^{(k)}(\mathbf{r})] \quad \text{for } i = 1, 2, \dots, n,$$

$$(41) \quad \tilde{\Phi}^{(k+1)}(\mathbf{r}) = \tilde{\Phi}^{(k)}(\mathbf{r}) + \omega [q(\mathbf{r}) - \tilde{\Phi}^{(k)}(\mathbf{r})],$$

where ω is a relaxation parameter, p_i is a solution of the nonlinear equation

$$(42) \quad g_i(p) = 0 \quad \text{with} \quad g_i(p) = p - a_i(\mathbf{r}) [1 - v_i \gamma p - b_i(\mathbf{r})]^{v_i/v_0},$$

and q is a solution of the finite element equation: Find $q \in \mathcal{M}_0$ such that

$$(43) \quad a(q, v) = \beta \sum_{i=1}^n Z_i \int_{D_s} c_i^{(k+1)} v d\mathbf{r} \quad \forall v \in \mathcal{M}_0.$$

Here, β is given in (12), γ in (22), a_i and b_i have been calculated via the expressions

$$(44) \quad a_i(\mathbf{r}) = c_i^b e^{-Z_i(\tilde{\Phi}^{(k)} + \Psi + G)}, \quad b_i(\mathbf{r}) = \gamma \left(\sum_{j=1}^{i-1} v_j c_j^{(k+1)} + \sum_{j=i+1}^n v_j c_j^{(k)} \right),$$

and the bilinear form $a(\cdot, \cdot)$ is defined in (25).

We terminate the iteration when the convergence rule is satisfied:

$$(45) \quad \max \left\{ \|\tilde{\Phi}^{(k+1)} - \tilde{\Phi}^{(k)}\|_{L^2(\Omega)}, \max_{1 \leq i \leq n} \|c_i^{(k+1)} - c_i^{(k)}\|_{L^2(\Omega)} \right\} < \tau,$$

where τ is a convergence tolerance ($\tau = 10^{-7}$ by default).

Each iteration of our nonlinear SOR-like scheme can be well defined as shown in Theorem 3.1.

Theorem 3.1. *The finite element equation (43) has a unique solution for any $c_i \in L^2(\Omega)$. If p satisfies the constraint conditions*

$$(46) \quad 0 \leq p \leq \frac{1 - b_i}{v_i \gamma}, \quad i = 1, 2, \dots, n,$$

where b_i is given in (44), then each nonlinear equation of (42) has a unique solution.

Proof. Since $a(\cdot, \cdot)$ is a symmetric bounded bilinear form, the first part of the theorem is obviously true [12]. We next find the derivative g'_i of g_i in the expression

$$(47) \quad g'_i(p) = 1 + \gamma \frac{v_i^2}{v_0} a_i(\mathbf{r}) [1 - \gamma v_i p - b_i(\mathbf{r})]^{v_i/v_0 - 1}, \quad i = 1, 2, \dots, n.$$

When p satisfies condition (46), it is clear that g_i and g'_i are well defined, and $g'_i > 0$. Thus, g_i is an increasing function. Clearly,

$$\lim_{p \rightarrow 0^+} g_i(p) = -a_i(1 - b_i)^{v_i/v_0} < 0, \quad g_i(p) \rightarrow 1 \text{ as } p \rightarrow \left(\frac{1 - b_i}{v_i \gamma}\right)^-.$$

Hence, each equation of (42) has a unique solution. \square

Because each equation of (42) is nonlinear, we solve it by the Newton scheme:

$$(48) \quad p_i^{(j+1)}(\mathbf{r}) = p_i^{(j)}(\mathbf{r}) - \frac{g_i(p^{(j)})}{g'_i(p^{(j)})}, \quad j = 0, 1, 2, 3, \dots,$$

for each interior mesh vertex of the mesh $\Omega_h \cap D_s$. Here the initial iterate $p_i^{(0)} = c_i^{(k)}$.

We terminate the Newton iteration and set $p_i = p_i^{(j+1)}$ for defining $c_i^{(k+1)}$ by (40) when the convergence rule is satisfied:

$$(49) \quad \|p_i^{(j+1)} - p_i^{(j)}\| \leq \tau_p,$$

where τ_p is a convergence tolerance, and $\|\cdot\|$ denotes the Euclidean vector norm on the mesh vertices of the mesh domain $\Omega_h \cap D_s$. By default, we set $\tau_p = 10^{-5}$.

As a special case, we simply set $p_i = p_i^{(1)}$ to yield the SOR-Newton method:

$$(50) \quad c_i^{(k+1)}(\mathbf{r}) = c_i^{(k)}(\mathbf{r}) - \omega \frac{g_i(c_i^{(k)})}{g'_i(c_i^{(k)})} \quad \text{for } i = 1, 2, \dots, n,$$

$$(51) \quad \tilde{\Phi}^{(k+1)}(\mathbf{r}) = \tilde{\Phi}^{(k)}(\mathbf{r}) + \omega [q(\mathbf{r}) - \tilde{\Phi}^{(k)}(\mathbf{r})].$$

For clarity, we summarize the above schemes in Algorithm 1.

Algorithm 1 (The nonuniform SMPBE finite element solver). *Let $(c_1, c_2, \dots, c_n, u)$ be a numerical solution of the nonuniform SMPBE model (34) defined on a Lagrange finite element space $\mathcal{M} \subset H^1(\Omega)$. It is calculated in four steps:*

Step 1: Calculate G via (14) and ∇G via (17) on \mathcal{M} .

Step 2: Find Ψ by the finite element solver from [56].

Step 3: Solve the nonlinear system (39) for $(c_1, c_2, \dots, c_n, \tilde{\Phi})$ by the nonlinear SOR-like (or SOR-Newton) iterative scheme as follows:

(1) Initialization: Set $k = 0$ and select $\tilde{\Phi}^{(0)}$ and $c_i^{(0)}$ for $i = 1, 2, \dots, n$.

(2) Calculate the updates $c_i^{(k+1)}$ for $i = 1, 2, \dots, n$ by (40) (or (50)).

(3) Calculate $\tilde{\Phi}^{(k+1)}$ by (41), where (43) is solved on \mathcal{M}_0 .

(4) Convergence test: If (45) holds, set $\tilde{\Phi} \approx \tilde{\Phi}^{(k+1)}$ and $c_i \approx c_i^{(k+1)}$ for $i = 1, 2, \dots, n$; otherwise, set $k := k + 1$, and return to (2).

Step 4: Construct u by the solution decomposition:

$$u(\mathbf{r}) = \tilde{\Phi}(\mathbf{r}) + \Psi(\mathbf{r}) + G(\mathbf{r}) \quad \text{on } \mathcal{M}.$$

4. A good selection of initial iterates

As nonlinear iterative methods, our nonlinear SOR-like and SOR-Newton schemes rely on a proper selection of initial iterate $\bar{c}^{(0)}$ for its convergence. To derive a good initial iterate, we consider a uniform ionic size case as follows:

$$v_i = \bar{v} \quad \text{with} \quad \bar{v} = \frac{1}{n} \sum_{j=1}^n v_j, \quad i = 1, 2, \dots, n.$$

By the binomial series $(1+x)^m = 1 + mx + O(x^2)$ for $|x| < 1$, we can obtain

$$\left(1 - \gamma \sum_{j=1}^n v_j c_j(\mathbf{r})\right)^{v_i/v_0} \approx 1 - \gamma \frac{\bar{v}^2}{v_0} \sum_{j=1}^n c_j(\mathbf{r}) \quad \forall \mathbf{r} \in D_s,$$

so that each nonlinear algebraic equation of (39) is approximated by

$$(52) \quad c_i - c_i^b w_i \left[1 - \gamma \frac{\bar{v}^2}{v_0} \sum_{j=1}^n c_j(\mathbf{r})\right] e^{-Z_i \tilde{\Phi}} = 0, \quad i = 1, 2, \dots, n.$$

We then can solve the above system for c_i to get that

$$(53) \quad c_i = \frac{c_i^b w_i e^{-Z_i \tilde{\Phi}(\mathbf{r})}}{1 + \gamma \frac{\bar{v}^2}{v_0} \sum_{j=1}^n w_j c_j^b e^{-Z_j \tilde{\Phi}}}, \quad i = 1, 2, \dots, n.$$

Substituting (53) to (16), we obtain a nonlinear interface boundary value problem for computing $\tilde{\Phi}$ as follows:

$$(54) \quad \begin{cases} \Delta \tilde{\Phi}(\mathbf{r}) = 0, & \mathbf{r} \in D_p, \\ \epsilon_s \Delta \tilde{\Phi}(\mathbf{r}) + \beta \frac{\sum_{i=1}^n Z_i c_i^b w_i(\mathbf{r}) e^{-Z_i \tilde{\Phi}(\mathbf{r})}}{1 + \gamma \frac{\bar{v}^2}{v_0} \sum_{i=1}^n c_i^b w_i(\mathbf{r}) e^{-Z_i \tilde{\Phi}(\mathbf{r})}} = 0, & \mathbf{r} \in D_s, \\ \tilde{\Phi}(\mathbf{s}^+) = \tilde{\Phi}(\mathbf{s}^-), \quad \epsilon_s \frac{\partial \tilde{\Phi}(\mathbf{s}^+)}{\partial \mathbf{n}(\mathbf{s})} = \epsilon_p \frac{\partial \tilde{\Phi}(\mathbf{s}^-)}{\partial \mathbf{n}(\mathbf{s})}, & \mathbf{s} \in \Gamma, \\ \tilde{\Phi}(\mathbf{s}) = 0, & \mathbf{s} \in \partial\Omega. \end{cases}$$

The above problem can be solved via our uniform SMPBE finite element solver [59] to yield an initial iterate $\tilde{\Phi}^{(0)}$. We then calculate the initial iterates $c_i^{(0)}$ by

$$(55) \quad c_i^{(0)}(\mathbf{r}) = \frac{c_i^b e^{-Z_i(\tilde{\Phi}^{(0)} + \Psi + G)}}{1 + \gamma \frac{\bar{v}^2}{v_0} \sum_{j=1}^n c_j^b e^{-Z_j(\tilde{\Phi}^{(0)} + \Psi + G)}}, \quad i = 1, 2, \dots, n.$$

Here, β is given in (12), and γ in (22).

5. Numerical results

We programmed Algorithm 1 as a software package, called nuSMPBE, in Python based on the state-of-the-art finite element library from the FEniCS project [39], the linear algebra library NumPy (<http://www.numpy.org>), and our PBE and uniform SMPBE program packages [27, 56, 59]. As a derived class, nuSMPBE inherits the parameters and methods from our PBE and uniform SMPBE software packages. Thus, a molecular surface-fitted tetrahedral mesh can be directly generated from nuSMPBE for each input PQR file of a protein. Here a PQR file is a modified protein data bank (PDB) file to include the hydrogen atoms (or some other atoms), the atomic charge numbers, and atomic radii that are missed in a PDB file

downloaded from the protein data bank (<http://www.rcsb.org>). It can be generated from the PDB2PQR web server (<http://nbc-222.ucsd.edu/pdb2pqr-2.1.1/>).

As usual, we treat each ion as a hard spherical ball with radius a_i to get

$$(56) \quad v_i = \frac{4\pi}{3}a_i^3, \quad i = 1, 2, \dots, n.$$

There are several selections of ionic radii [9, 11, 63]. In our tests, we used the ionic radii from one classic textbook for *Physical Chemistry* [9, Table 11.3, page 330]. We also selected the bulk concentrations c_i^b according to the electroneutrality condition

$$(57) \quad \sum_{i=1}^n Z_i c_i^b = 0,$$

and calculated the ionic strength I_s by the formula $I_s = \frac{1}{2} \sum_{i=1}^n (Z_i)^2 c_i^b$. Here I_s and c_i^b are given in mol/L.

Furthermore, we used the linear order of finite element method, and solved each related finite element equation via the preconditioned conjugate gradient method using incomplete LU preconditioning from the PETSc library [6] with the relative or the absolute residual norm being less than 10^{-8} .

For the purpose of demonstrating the convergence and performance of our new SMPBE finite element solvers, we did numerical tests for a symmetric 1:1 ionic solvent in which the table salt (NaCl) dissolves into sodium ions (Na^+) and chloride ions (Cl^-) in water. In these tests ($n = 2$), c_1 and c_2 denoted the concentrations of Na^+ and Cl^- , respectively, $Z_1 = 1$, $Z_2 = -1$, $a_1 = 0.95 \text{ \AA}$, and $a_2 = 1.81 \text{ \AA}$. According to (57), we set $c_1^b = c_2^b = I_s$.

We also did tests on a molten salt (NaCl + KCl) solution [32]. In these tests, c_1 , c_2 , and c_3 represented the concentrations of Na^+ , Cl^- , and K^+ , respectively. To satisfy (57), we set $c_1^b = 3I_s/4$, $c_2^b = I_s$, and $c_3^b = I_s/4$. The radius of a potassium ion (K^+) was set as $a_3 = 1.33 \text{ \AA}$.

In these numerical tests, we set the boundary value function $\hat{g} = 0$ for simplicity. The purpose of these tests is to demonstrate the convergence and performance of our nonlinear SOR-like scheme (i.e., each nonlinear equation was solved by the Newton method until the convergence rule (49) was satisfied) and our SOR-Newton scheme (i.e., each nonlinear equation was solved by one Newton iteration only). All the numerical tests were done on our Mac Pro Workstation with 3.7 GHz Quad-Core Intel Xeon E5 processor and 64 GB memory.

5.1. Validation tests on a Born ball model. We construct a Born ball test model with $D_p = \{\mathbf{r} \mid |\mathbf{r}| < a\}$, $\Omega = \{\mathbf{r} \mid |\mathbf{r}| < A\}$, $\Gamma = \{\mathbf{r} \mid |\mathbf{r}| = a\}$, and $D_s = \{\mathbf{r} \mid a < |\mathbf{r}| < A\}$, where a and A are two positive numbers satisfying $A > a$, and D_s contains the table salt solution (i.e., $n = 2$, $Z_1 = 1$, $Z_2 = -1$, $a_1 = 0.95$, $a_2 = 1.81$, and $c_1^b = c_2^b = I_s$). One point charge, ze_c , is placed in the center of D_p to yield an electrostatic potential and two concentration functions that are spherically symmetric. It is this physical property that makes the Born ball test model valuable for validating either a dielectric continuum model or a numerical solver, in the case of not knowing any analytical solution.

In the numerical tests, we set $a = 17$, $A = 51$, $z = 10$, $I_s = 0.2$, and $\omega = 0.45$. We then constructed three nested interface fitted tetrahedral meshes with 3134, 25131, and 200009 vertices to validate the convergence of nonuniform SMPBE finite element solutions. Here, the nonlinear SOR-like iterative scheme was used to solve the nonuniform SMPBE. All the values of the electrostatic potential function u and

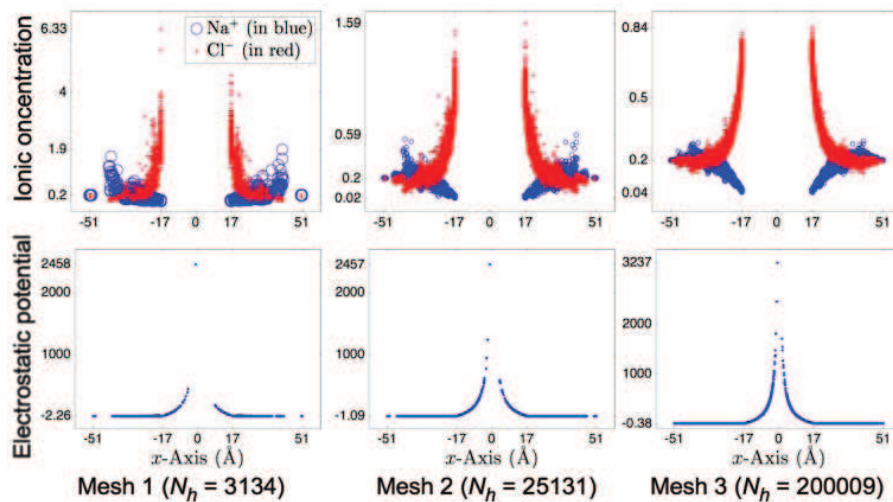


FIGURE 2. Convergence tendency of the electrostatic potential function u and ionic concentration functions c_1 (for sodium ions in the blue color) and c_2 (for chloride ions in the red color) produced by our nonlinear SOR-like iterative scheme for the Born ball model with a positive central charge, $10e_c$, on three nested irregular meshes. Here N_h is the number of mesh vertices.

two concentration functions c_1 (for sodium ions) and c_2 (for chloride ions) on the mesh vertices were plotted along the x -axis in Figure 2.

From Figure 2 it can be seen that the numerical solutions of c_1 , c_2 , and u kept the spherical symmetry well. As expected in physics, the concentrations of sodium and chloride ions (c_1 and c_2) decrease and increase, respectively, when mesh vertices move from the boundary $\partial\Omega$ to the interface Γ due to the positive central point charge number, $z = 10$. As the number of mesh vertices was increased from 3134 to 200009, the ranges of ionic concentration functions c_1 and c_2 were decreased monotonically while the range of potential function u was increased monotonically, as shown in the numbers marked on the y -axis, indicating the convergence of the finite element solutions to the exact solution of the nonuniform SMPBE.

5.2. Convergence and performance. We made tests on a protein (PDB ID: 4PTI) with 892 atoms to demonstrate the convergence and performance of our nonlinear SOR-like and SOR-Newton schemes. In these tests, two different molecular surfaces, called the solvent-excluded surface (SES) and Gaussian surface, were selected for defining the interface Γ between the protein and solvent regions. By our software nSMPBE with the default mesh parameter values, SES and Gaussian interface fitted irregular tetrahedral meshes were generated with 24969 and 67582 mesh vertices, respectively. As shown in Figure 3, SES is much more irregular and bumpier than Gaussian surface. Thus, the SES mesh resulted in a good test case for us to check the robustness of our nonlinear SOR-like and SOR-Newton schemes. A part of the SES mesh domain Ω_h is displayed in Figure 4.

In the tests, the bulk concentrations were set as $c_1^b = 0.1$ and $c_2^b = 0.1$. Two initial iterates and the SES and Gaussian mesh domains were used in the tests. The numerical results were reported in Tables 1 and 2 and Figure 5. Here I_{te}

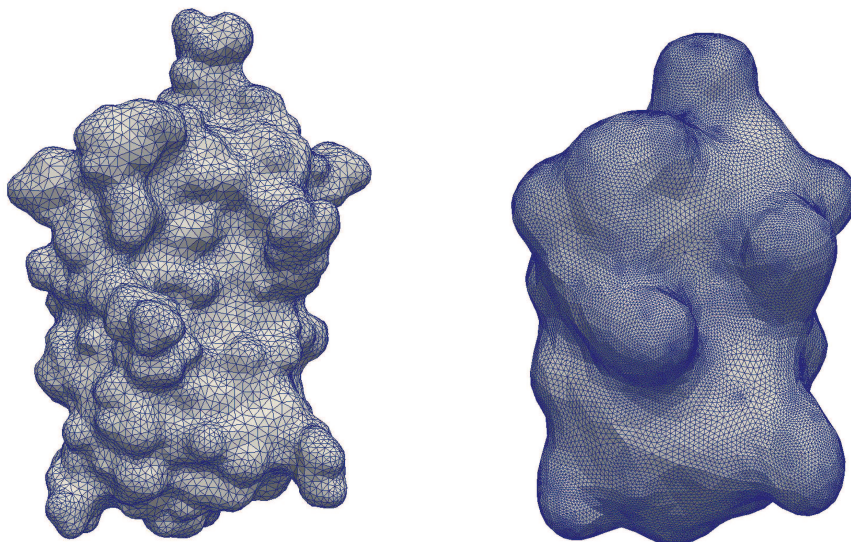


FIGURE 3. A solvent excluded molecular surface (left) [60] and a Gaussian molecular surface (right) [62] for a protein (PBE ID: 4PTI) for the numerical tests reported in Tables 1 and 2.

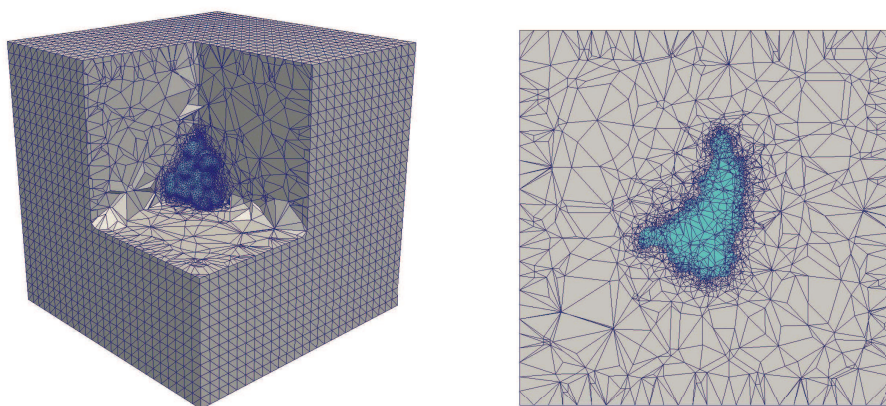


FIGURE 4. An interface fitted irregular tetrahedral mesh domain Ω_h with 24969 mesh vertices for the protein (PBE ID: 4PTI) with 892 atoms. Here one corner of the cubic domain is removed to display the mesh surrounding the protein. A cross-section of the mesh domain is displayed in the right plot.

denotes the total number of iterations satisfying the convergence rule (45), CPU is the computer time spent for solving the nonuniform SMPBE system, and N_h is the total number of mesh vertices of Ω_h . In these tests, the convergence tolerance of (45) was set as $\tau = 10^{-7}$.

Tables 1 and 2 show that the two finite element solvers worked efficiently, and the initial iterates generated from the improved uniform SMPBE (54) significantly enhanced the two solvers in both convergence and performance in comparison to the cases using the simple zero initial iterate in solving for $\tilde{\Phi}$. Here the CPU time data

TABLE 1. A comparison of the performance of our nonlinear SOR-like scheme with that of our SOR-Newton scheme for the protein (PDB ID: 4PTI) in the case of using initial iterate $\tilde{\Phi}^{(0)} = 0$.

(1) Performance with $N_h = 24969$ and $\tilde{\Phi}^{(0)} = 0$ (in minutes)								
The nonlinear SOR scheme (40)					The SOR-Newton scheme (50)			
ω	0.05	0.1	0.15	0.2	0.05	0.1	0.15	0.2
Ite.	368	194	132	Fail	502	255	171	128
CPU	1.64	1.17	0.81		2.22	1.12	0.90	0.62
(2) Performance with $N_h = 67582$ and $\tilde{\Phi}^{(0)} = 0$ (in minutes)								
The nonlinear SOR scheme (40)					The SOR-Newton scheme (50)			
ω	0.05	0.1	0.15	0.2	0.05	0.1	0.15	0.2
Ite.	378	193	128	Fail	418	208	144	120
CPU	9.42	4.86	3.21		10.42	5.19	3.53	2.73

TABLE 2. A comparison of the performance of our nonlinear SOR-like scheme with that of our SOR-Newton scheme for the protein (PDB ID: 4PTI) in the case of using an initial iterate $\tilde{\Phi}^{(0)}$ defined by a numerical solution of the improved uniform SMPBE (54).

(1) Performance with $N_h = 24969$ and $\tilde{\Phi}^{(0)}$ defined by (54) (in minutes)										
The nonlinear SOR scheme (40)										
ω	0.05	0.1	0.15	0.2	0.25	0.3	0.35	0.4	0.45	0.5
Ite.	327	173	118	89	71	59	50	43	39	Fail
CPU	1.51	0.98	0.77	0.59	0.47	0.36	0.32	0.28	0.26	
The nonlinear SOR-Newton scheme (50)										
Ite.	502	255	171	128	102	84	72	62	55	Fail
CPU	2.24	1.15	0.89	0.66	0.53	0.44	0.39	0.34	0.30	
(2) Performance with $N_h = 67582$ and $\tilde{\Phi}^{(0)}$ defined by (54) (in minutes)										
The nonlinear SOR scheme (40)										
Ite.	306	162	109	83	65	54	46	40	35	32
CPU	7.66	4.26	2.94	2.28	1.83	1.45	1.25	1.11	0.99	0.92
The nonlinear SOR-Newton scheme (50)										
Ite.	363	180	117	89	70	59	49	42	36	33
CPU	9.28	4.70	3.11	2.29	1.80	1.53	1.27	1.04	0.92	0.86

did not include the time spent on the calculation of initial iterates defined by (54) and (55) (i.e., solving the improved uniform SMPBE), which were about 3 and 12 seconds, respectively, on the meshes with 24969 and 67582 vertices. With an initial iterate generated from our improved uniform SMPBE, the two finite element solvers worked with a larger relaxation parameter of ω and a faster rate of convergence. For example, the SOR-Newton scheme using $\omega = 0.5$ took only 33 iterations in about 0.86 minutes to find the solution of the nonuniform SMPBE system (39), which consists of $\tilde{\Phi}$ and the two ionic concentrations c_1 and c_2 , on an irregular mesh of 67582 mesh vertices.

Figure 5 displays the convergence behavior of our nonlinear SOR-like and SOR-Newton schemes for the protein (4PTI) case. From it we see that the SOR-Newton scheme can have a rate of convergence close to the nonlinear SOR-like scheme.

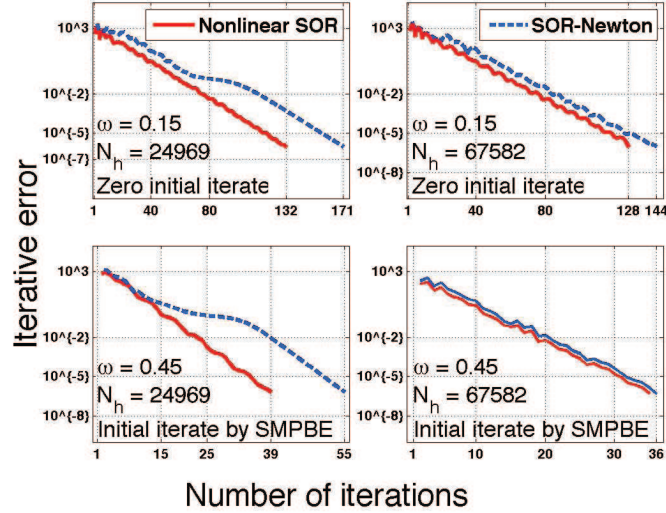


FIGURE 5. A comparison of the convergence of the nonlinear SOR-like scheme with that of the SOR-Newton scheme for the protein (4PTI) using two different initial iterates. Here the iterative error equals $\max\{\|\tilde{\Phi}^{(k+1)} - \tilde{\Phi}^{(k)}\|_{L^2(\Omega)}, \max_{1 \leq i \leq n} \|c_i^{(k+1)} - c_i^{(k)}\|_{L^2(D_s)}\}$.

Figure 5 also confirms the importance of selecting a good initial iterate in the implementation of our nonlinear SOR-like and SOR-Newton schemes.

Figure 6 displays the color mapping of the electrostatic potential u and the concentrations, c_1 for Na^+ and c_2 for Cl^- , predicted by our nonlinear SOR-like scheme on a cross section of the mesh domain Ω_h with 67582 mesh vertices. From the figure it can be seen that the predicted values of c_1 and c_2 match reasonably to the distribution of u and the charge neutrality condition (57). In the area accumulated with the anions (Cl^-), cations (Na^+) were repelled away, causing the electrostatic potential u to have positive values.

TABLE 3. Performance of our nonlinear SOR-like and SOR-Newton schemes for solving the nonlinear system (39) for the protein (4PTI) in the NaCl-KCl solution.

Scheme	ω	Ite.	CPU (in minutes)
Born ball test model on mesh with $N_h = 200009$			
SOR-like	0.45	24	1.69
SOR-Newton	0.45	26	1.81
Protein (4PTI) on mesh with $N_h = 24969$			
SOR-like	0.42	129	1.04
SOR-Newton	0.42	93	0.51
Protein (4PTI) on mesh with $N_h = 67582$			
SOR-like	0.45	36	0.88
SOR-Newton	0.45	37	0.89

solving the nonlinear system (39)

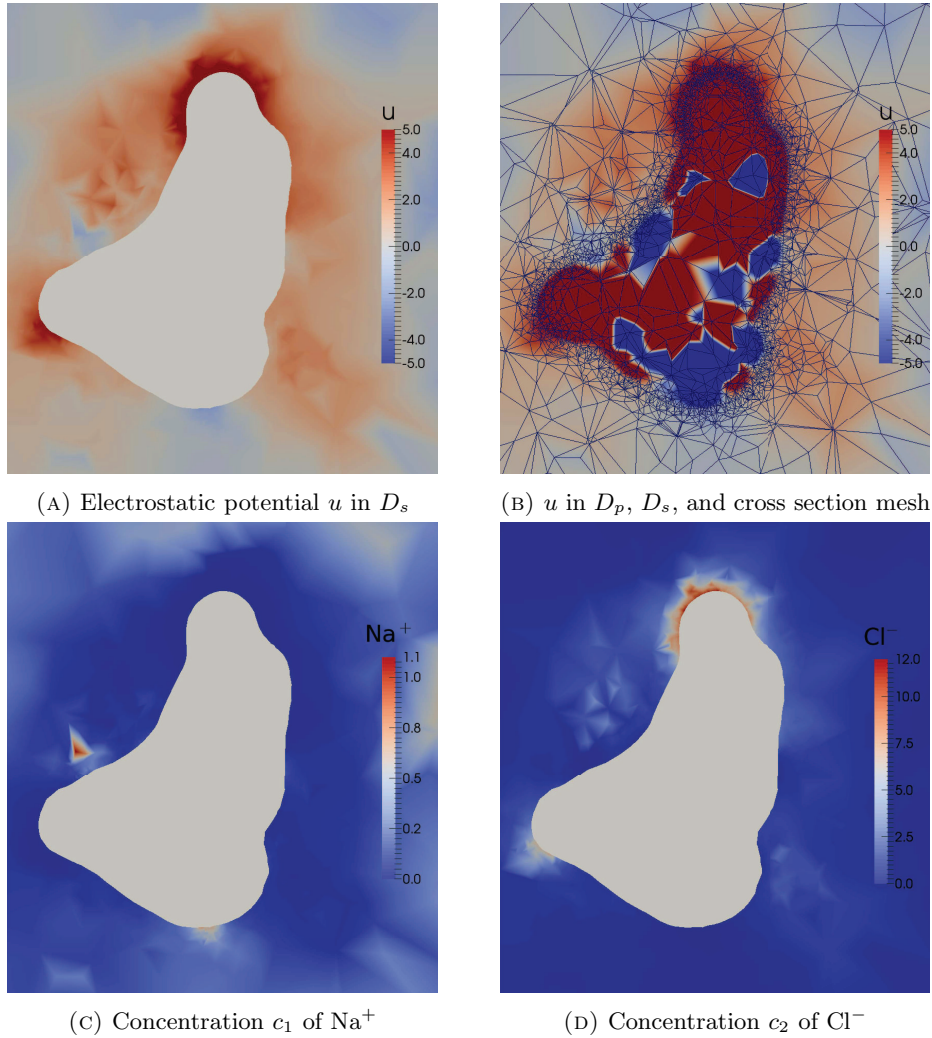


FIGURE 6. Color mappings of u , c_1 , and c_2 onto a cross section of mesh domain Ω_h on the yz coordinate plane. Here, $c_1 = c_2 = 0$ in the protein region D_p (in the white color), and the mapping of u has been rescaled to the range $[-5, 5]$ to increase the color contrast.

5.3. Performance for protein in NaCl-KCl solution. We did tests on a NaCl-KCl solution using $I_s = 0.2$, $c_1^b = 0.15$, $c_2^b = 0.2$, $c_3^b = 0.05$ (in mol/L), $a_1 = 0.95$, $a_2 = 1.81$, and $a_3 = 1.33$ (in \AA). The numerical solution of the nonuniform SMPBE (34) gave four functions — one electrostatic potential u and three concentrations: c_1 for sodium ions (Na^+), c_2 for chloride ions (Cl^-), and c_3 for potassium ions (K^+). We used the nonlinear SOR-like scheme (40) and the SOR-Newton scheme (50) to solve the nonlinear system (39) in the cases of the Born ball test model and the protein (4PTI). The test results were reported in Table 3, demonstrating that these two schemes worked efficiently.

We finally plotted the electrostatic potential function u and three ionic concentration functions from the Born ball test model in Figure 7. From this figure it can be seen that the four numerical functions of u and c_i for $i = 1, 2, 3$ kept the spherical

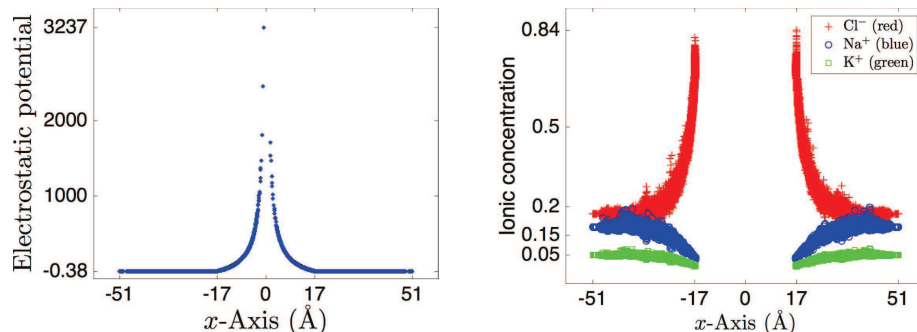


FIGURE 7. The electrostatic potential u (on the left plot) and the ionic concentrations c_1, c_2 , and c_3 (on the right plot) of sodium ions Na^+ , chloride ions Cl^- , and potassium ions K^+ produced by the nonlinear SOR-like scheme for the Born ball test model with central charge $10e_c$ in the NaCl-KCl solution. Here the bulk concentrations $c_1^b = 0.15$, $c_2^b = 0.2$, $c_3^b = 0.05$ mol/L.

symmetry of the Born ball test model solution. The concentration c_1 of Na^+ ions has the same pattern as the concentration c_3 of K^+ while its values are almost three times larger than the values of c_3 because the bulk concentration $c_1^b = 3c_3^b$. These test results partially validated the numerical results generated from our SOR-like iterative scheme.

6. Conclusions

We have presented two new nonuniform SMPBE finite element solvers using solution decomposition and nonlinear SOR iterative techniques, and programmed them as a software package for a protein in a solvent with multiple ionic species in distinct sizes. Their mathematical and numerical properties have been studied theoretically and numerically. We also proposed an improved uniform SMPBE, and used it to produce good initial iterates for our two new iterative schemes — the nonlinear SOR-like scheme and the SOR-Newton scheme. Numerical results on a Born ball test model and a protein in NaCl and NaCl-KCl solutions validated the new nonuniform SMPBE finite element solvers, and demonstrated the high performance of the new software package.

Furthermore, we have presented a new derivation of the nonuniform SMPBE, along with a detailed discription of a general Poisson dielectric model. This part of the paper is particularly valuable for us to study SMPBE models. Because of using solution decomposition techniques and a new electrostatic free energy functional, our new derivation and analysis of the nonuniform SMPBE have avoided the drawbacks of the traditional derivations and analyses caused by using the traditional electrostatic free energy functional that involves the singular electrostatic potential function, the concentration of water molecules, and the volume of a water molecule. Our new derivation has yielded a new nonuniform SMPBE. The difference between our new nonuniform SMPBE and the current ones can be seen from a comparison of our equilibrium equation (30) with the one given in [42, eq. (25) on page 2479] or the one given in [33, eq. (3.4) on page 819].

Our nonuniform SMPBE software package will be a valuable tool for us to study the effects of nonuniform ion sizes on the structure and function of a protein molecule and on the electrostatic solvation and binding free energies. It also enables

us to carry out various validation tests by using experiment data from chemical and biological laboratories. Moreover, we can use it do comparison tests with other SMPBE solvers (e.g., the one from [14]), and to address some questions arisen from the current SMPBE studies such as the one from [55] on the differences between SMPBE and a PBE Stern layer correction model. These research issues will be studied in our sequential papers.

Acknowledgements

This work was partially supported by the National Science Foundation, USA, through grant DMS-1226259. The author thanks Dr. Yi Jiang for his help with program writing and figure plotting. He also thanks the two reviewers for their valuable comments.

References

- [1] R. A. Adams and J. F. Fournier. Sobolev Spaces, volume 140 of Pure and Applied Mathematics. Amsterdam). Elsevier/Academic Press, Amsterdam, second edition, 2003.
- [2] J. Antosiewicz, J. A. McCammon, and M. K. Gilson. Prediction of pH-dependent properties of proteins. *J Mol Biol*, 238(3):415–36, 1994.
- [3] N. A. Baker. Poisson-Boltzmann methods for biomolecular electrostatics. *Methods in Enzymology*, 383:94–118, 2004.
- [4] N. A. Baker. Improving implicit solvent simulations: a Poisson-centric view. *Curr. Opin. Struc. Biol.*, 15:137–143, 2005.
- [5] N. A. Baker, D. Sept, M. Holst, and J. A. McCammon. The adaptive multilevel finite element solution of the Poisson-Boltzmann equation on massively parallel computers. *IBM Journal of Research and Development*, 45:427–438, 2001.
- [6] S. Balay, J. Brown, K. Buschelman, V. Eijkhout, W.D. Gropp, D. Kaushik, M.G. Knepley, L.C. McInnes, B.F. Smith, and H. Zhang. PETSc users manual. Technical Report ANL-95/11 - Revision 3.1, Argonne National Laboratory, 2010.
- [7] N. Ben-Tal, A. Ben-Shaul, A. Nicholls, and B. H. Honig. Free energy determinants of alpha-helix insertion into lipid bilayers. *Biophys. J.*, 70:1803–1812, 1996.
- [8] S. Berneche, M. Nina, and B. Roux. Molecular dynamics simulation of melittin in a dimyristoylphosphatidylcholine bilayer membrane. *Biophysical Journal*, 75:1603–1618, 1998.
- [9] R. S. Berry, S. A. Rice, and J. Ross. *Physical Chemistry*. Wiley, New York, NY, 1980.
- [10] I. Borukhov, D. Andelman, and H. Orland. Steric effects in electrolytes: A modified Poisson-Boltzmann equation. *Physical Review Letters*, 79(3):435–438, 1997.
- [11] A. H. Boschitsch and P.V. Danilov. Formulation of a new and simple nonuniform size-modified Poisson-Boltzmann description. *Journal of Computational Chemistry*, 33:1152–1164, 2012.
- [12] S. C. Brenner and L. R. Scott. *The Mathematical Theory of Finite Element Methods*. Springer-Verlag, New York, third edition, 2008.
- [13] D. Chen, Z. Chen, C. Chen, W. Geng, and G. Wei. MIBPB: A software package for electrostatic analysis. *Journal of Computational Chemistry*, 32(4):756–770, 2011.
- [14] V. B. Chu, Y. Bai, J. Lipfert, D. Herschlag, and S. Doniach. Evaluation of ion binding to DNA duplexes using a size-modified Poisson-Boltzmann theory. *Biophysical Journal*, 93(9):3202–3209, 2007.
- [15] M. E. Davis, J. D. Madura, B. A. Luty, and J. A. McCammon. Electrostatics and diffusion of molecules in solution: Simulations with the University of Houston Brownian dynamics program. *Comp. Phys. Comm.*, 62:187–197, 1991.
- [16] M. E. Davis and J. A. McCammon. Solving the finite difference linearized Poisson-Boltzmann equation: A comparison of relaxation and conjugate gradient methods. *J. Comp. Chem.*, 10:386–391, 1989.
- [17] M. E. Davis and J. A. McCammon. Electrostatics in biomolecular structure and dynamics. *Chem. Rev.*, 90:509–521, 1990.
- [18] P. Debye. *Polar Molecules*. Dover, New York, 1945.
- [19] F. Fogolari, A. Brigo, and H. Molinari. The Poisson-Boltzmann equation for biomolecular electrostatics: A tool for structural biology. *J. Mol. Recognit.*, 15(6):377–392, 2002.
- [20] D. Gillespie. A review of steric interactions of ions: Why some theories succeed and others fail to account for ion size. *Microfluidics and Nanofluidics*, 18:717–738, 2015.

- [21] M. K. Gilson and B. H. Honig. Energetics of charge-charge interactions in proteins. *Proteins*, 3(1):32–52, 1988.
- [22] D. J. Griffiths. *Introduction to Electrodynamics*. Prentice Hall, New Jersey, 3 edition, 1999.
- [23] M. J. Holst. *The Poisson-Boltzmann equation: Analysis and multilevel numerical solution*. Technical report, Applied Mathematics and CRPC, California Institute of Technology, 1994.
- [24] B. Honig and A. Nicholls. Classical electrostatics in biology and chemistry. *Science*, 268:1144–1149, May 1995.
- [25] A. L. Hovarth. *Handbook of aqueous electrolyte solutions: physical properties, estimation, and correlation methods*. Ellis Horwood, New York, 1985.
- [26] Y. Jiang, J. Ying, and D. Xie. A Poisson-Boltzmann equation test model for protein in spherical solute region and its applications. *Molecular Based Mathematical Biology*, 2:86–97, 2014. Open Access.
- [27] Y. Jiang, Y. Xie, J. Ying, D. Xie, and Z. Yu. SDPBS web server for calculation of electrostatics of ionic solvated biomolecules. *Molecular Based Mathematical Biology*, 3:179–196, 2015.
- [28] D. J.-Morales, J. Liang, and B. Eisenberg. Ionizable side chains at catalytic active sites of enzymes. *European Biophysics Journal*, 41(5):449–460, 2012.
- [29] S. Jo, M. Vargyas, J. Vasko-Szedlar, B. Roux, and W. Im. PBEQ-solver for online visualization of electrostatic potential of biomolecules. *Nucleic Acids Research*, 36(suppl 2):W270–W275, 2008.
- [30] P. Koehl and M. Delarue. AQUASOL: an efficient solver for the dipolar Poisson-Boltzmann-Langevin equation. *The Journal of Chemical Physics*, 132(6):064101, 2010.
- [31] W. Kunz. *Specific Ion Effects*. World Scientific, Singapore, 2009.
- [32] B. Larsen, T. Førland, and K. Singer. A Monte Carlo calculation of thermodynamic properties for the liquid NaCl+ KCl mixture. *Molecular Physics*, 26(6):1521–1532, 1973.
- [33] B. Li. Continuum electrostatics for ionic solutions with non-uniform ionic sizes. *Nonlinearity*, 22(4):811–833, April 2009.
- [34] B. Li. Minimization of electrostatic free energy and the Poisson-Boltzmann equation for molecular solvation with implicit solvent. *SIAM J. Math. Anal.*, 40(6):2536–2566, 2009.
- [35] B. Li, P. Liu, Z. Xu, and S. Zhou. Ionic size effects: generalized Boltzmann distributions, counterion stratification and modified Debye length. *Nonlinearity*, 26(10):2899, 2013.
- [36] J. Li and D. Xie. An effective minimization protocol for solving a size-modified Poisson-Boltzmann equation for biomolecule in ionic solvent. *International Journal of Numerical Analysis and Modeling*, 12(2):286–301, 2015.
- [37] J. Li and D. Xie. A new linear Poisson-Boltzmann equation and finite element solver by solution decomposition approach. *Communications in Mathematical Sciences*, 13(2):315–325, 2015.
- [38] J. Liu and B. Eisenberg. Numerical methods for a Poisson-Nernst-Planck-Fermi model of biological ion channels. *Physical Review E*, 92(1):012711, 2015.
- [39] A. Logg, K.-A. Mardal, and G. N. Wells, editors. *Automated Solution of Differential Equations by the Finite Element Method*, volume 84 of *Lecture Notes in Computational Science and Engineering*. Springer Verlag, 2012.
- [40] B. Lu, X. Cheng, J. Huang, and J. A. McCammon. AFMPB: An adaptive fast multipole Poisson-Boltzmann solver for calculating electrostatics in biomolecular systems. *Computer Physics Communications*, 181:1150–1160, 2010.
- [41] B. Lu, Y. Zhou, M.J. Holst, and J.A. McCammon. Recent progress in numerical methods for the Poisson-Boltzmann equation in biophysical applications. *Commun. Comput. Phys.*, 3(5):973–1009, 2008.
- [42] B. Lu and Y. Zhou. Poisson-Nernst-Planck equations for simulating biomolecular diffusion-reaction processes II: size effects on ionic distributions and diffusion-reaction rates. *Biophysical Journal*, 100(10):2475–2485, 2011.
- [43] R. Luo, L. David, and M. K Gilson. Accelerated Poisson-Boltzmann calculations for static and dynamic systems. *Journal of Computational Chemistry*, 23(13):1244–1253, 2002.
- [44] M. Nina, D. Beglow, and B. Roux. Atomic radii for continuum electrostatics calculations based on molecular dynamics free energy simulations. *J. Phys. Chem. B*, 101:5239–?, 1997.
- [45] J. M. Ortega and W. C. Rheinboldt. *Iterative Solution of Nonlinear Equations in Several Variables*. Academic Press, 1970.
- [46] K. S. Pitzer. *Activity Coefficients in Electrolyte Solutions*. CRC Press, Boca Raton FL USA, 1991.

- [47] Y. Qiao, X. Liu, M. Chen, and B. Lu. A local approximation of fundamental measure theory incorporated into three dimensional Poisson-Nernst-Planck equations to account for hard sphere repulsion among ions. *Journal of Statistical Physics*, 163(1):156–174, 2016.
- [48] P. Ren, J. Chun, D. G. Thomas, M. J. Schnieders, M. Marucho, J. Zhang, and N. A. Baker. Biomolecular electrostatics and solvation: a computational perspective. *Quarterly Reviews of Biophysics*, 45(04):427–491, 2012.
- [49] W. Rocchia, E. Alexov, and B. Honig. Extending the applicability of the nonlinear Poisson-Boltzmann equation: Multiple dielectric constants and multivalent ions. *J. Phys. Chem. B*, 105:6507–6514, 2001.
- [50] B. Roux and T. Simonson. Implicit solvent models. *Biophys. Chem.*, 78:1–20, 1999.
- [51] S. Subramaniam. Treatment of electrostatic effects in proteins: Multigrid-based Newton iterative method for solution of the full nonlinear Poisson-Boltzmann equation. *Prot. Struct. Func. Gen.*, 18:231–245, 1994.
- [52] R. C. Tan, T.N. Truong, and J.A. McCammon. Acetylcholinesterase: Electrostatic steering increases the rate of ligand binding. *Biochemistry*, 32:401–403, 1993.
- [53] C. L. Vizcarra and S. L. Mayo. Electrostatics in computational protein design. *Current Opinion in Chemical Biology*, 9:622–626, 2005.
- [54] C. Wang, J. Wang, Q. Cai, Z. Li, H.-K. Zhao, and R. Luo. Exploring accurate Poisson-Boltzmann methods for biomolecular simulations. *Computational and Theoretical Chemistry*, 1024:34–44, 2013.
- [55] N. Wang, S. Zhou, P. M Kekenus-Huskey, B. Li, and J. A. McCammon. Poisson-Boltzmann versus size-modified Poisson-Boltzmann electrostatics applied to lipid bilayers. *The Journal of Physical Chemistry B*, 118(51):14827–14832, 2014.
- [56] D. Xie. New solution decomposition and minimization schemes for Poisson-Boltzmann equation in calculation of biomolecular electrostatics. *J. Comput. Phys.*, 275:294–309, 2014.
- [57] D. Xie and J. Li. A new analysis of electrostatic free energy minimization and Poisson-Boltzmann equation for protein in ionic solvent. *Nonlinear Analysis: Real World Applications*, 21:185–196, 2015.
- [58] D. Xie, H. W. Volkmer, and J. Ying. Analytical solutions of nonlocal Poisson dielectric models with multiple point charges inside a dielectric sphere. *Physical Review E*, 93(4):043304, 2016.
- [59] Y. Xie, J. Ying, and D. Xie. SMPBS: Web server for computing biomolecular electrostatics using finite element solvers of size modified Poisson-Boltzmann equation. *Journal of Computational Chemistry*, 38(8):541–552, 2017.
- [60] D. Xu and Y. Zhang. Generating triangulated macromolecular surfaces by Euclidean distance transform. *PloS ONE*, 4(12):e8140, 2009.
- [61] J. Ying and D. Xie. A new finite element and finite difference hybrid method for computing electrostatics of ionic solvated biomolecule. *Journal of Computational Physics*, 298:636–651, 2015.
- [62] Z. Yu, M.J. Holst, Y. Cheng, and J.A. McCammon. Feature-preserving adaptive mesh generation for molecular shape modeling and simulation. *Journal of Molecular Graphics and Modelling*, 26(8):1370–1380, 2008.
- [63] S. Zhou, Z. Wang, and B. Li. Mean-field description of ionic size effects with nonuniform ionic sizes: A numerical approach. *Physical Review E*, 84(2):021901, 2011.

Dexuan Xie, Department of Mathematical Sciences, University of Wisconsin-Milwaukee, Milwaukee, WI 53201-0413, USA

E-mail: dxie@uwm.edu

URL: <http://www.uwm.edu/~dxie>